Cite this article
Kao GTC, Iannuzzo A, Coros S, Van Mele T and Block P
Understanding the rigid-block equilibrium method by way of mathematical programming.
Proceedings of the Institution of Civil Engineers – Engineering and Computational Mechanics,
https://doi.org/10.1680/jencm.20.00036

Research Article
Paper 2000036
Received 29/09/2020;
Accepted 02/03/2021

Keywords: computational mechanics/masonry/limit equilibrium methods

Engineering and Computational Mechanics

ice Publishing

Understanding the rigid-block equilibrium method by way of mathematical programming

Gene Ting-Chun Kao MSc
PhD Researcher, Department of Architecture, Institute of Technology in Architecture, Block Research Group, Eidgenössische Technische Hochschule Zürich (ETH Zurich), Zurich, Switzerland (Orcid:0000-0002-4275-1246)

Antonino Iannuzzo PhD
Postdoctoral Researcher, Department of Architecture, Institute of Technology in Architecture, Block Research Group, Eidgenössische Technische Hochschule Zürich (ETH Zurich), Zurich, Switzerland (Orcid:0000-0002-6633-149X) (corresponding author: iannuzzo@arch.ethz.ch)

Stelian Coros PhD
Assistant Professor, Department of Computer Science, Institute for Pervasive Computing, Computational Robotics Lab, Eidgenössische Technische Hochschule Zürich (ETH Zurich), Zurich, Switzerland (Orcid:0000-0001-6604-4784)

Tom Van Mele PhD
Senior Scientist, Department of Architecture, Institute of Technology in Architecture, Block Research Group, Eidgenössische Technische Hochschule Zürich (ETH Zurich), Zurich, Switzerland (Orcid:0000-0002-4614-1808)

Philippe Block PhD
Full Professor, Department of Architecture, Institute of Technology in Architecture, Block Research Group, Eidgenössische Technische Hochschule Zürich (ETH Zurich), Zurich, Switzerland (Orcid:0000-0003-2355-0614)

This paper discusses and extends some main features of the rigid-block equilibrium (RBE) method. RBE is a numerical approach that frames the equilibrium problem of rigid-block assemblies as an optimisation problem to compute possible internal and equilibrated singular stress states. The contact between blocks is considered having a finite friction capacity and the unilateral behaviour is modelled through a penalty formulation. In particular, the penalty formulation widens the standard admissible solution space of compressive-only forces by allowing for tensile forces appearing on potentially unstable regions. The RBE objective function minimises the interface forces whereas the constraints are linear functions enforcing the static equilibrium of the whole assembly. In this paper, along with the original quadratic objective function, the authors propose a linear function to illustrate and explore the role played by both the nodal forces and the interface resultants. Moreover, the authors show how RBE can be used to explore different admissible internal stress states – for example, due to increasing, static, horizontal actions.

Notation

A	zero-order area moment
$\mathbf{A}_{\text{eq}}$	equilibrium matrix
$\mathbf{A}_{\text{fr}}$	matrix enforcing the linearised Mohr–Coulomb yield criterion
$\mathbf{c}$	vector collecting the weighting factors attributed to the compressive, tensile and friction forces
E	edges of the graph $G(V, E)$
$\mathbf{f}$	vector collecting the nodal forces
$\boldsymbol{f}_k^i$	i-th nodal force of the kth interface
$\left(f_{kn}^i,\ f_{ku}^i,\ f_{kv}^i\right)$	components of the nodal forces in the interface local reference system
f_{kn}^{i+}	positive part of the normal component f_{kn}^i
f_{kn}^{i-}	negative part of the normal component f_{kn}^i
$\boldsymbol{f}_{\text{LP}}^*$	solution of the linear optimisation problem
$\boldsymbol{f}_{\text{QP}}^*$	solution of the quadratic optimisation problem
$G(V, E)$	graph representing the assembly data structures
$\mathbf{H}$	diagonal matrix: diag($\boldsymbol{c}$)
$\mathbf{J}_0$	second-order area moment
$\boldsymbol{n}_i$	unit outward normal
$(\hat{\boldsymbol{n}}_k,\ \hat{\boldsymbol{u}}_k,\ \hat{\boldsymbol{v}}_k)$	standard basis defining the local reference system of the kth interface
$\mathbf{p}$	vector collecting the external forces
$\boldsymbol{R}$	second-order, skew-symmetric tensor that rotates in the positive direction of any vector by $\pi/2$
$\mathbf{r}_i$	position vector of the ith vertex
$\mathbf{S}_0$	first-order area moment
$\mathbf{V}$	vector storing the vertices of the graph $G(V, E)$
$\boldsymbol{v}_k^i$	ith vertex of the kth interface
μ	friction coefficient
Ω	planar, polygonal interface between two blocks

1. A brief introduction to rigid-block equilibrium method

The use of safe theorem of limit analysis, as proved by Heyman (1966), is a wide-spread approach to assess masonry structures. It states that a structure is safe if an admissible stress state can be found in equilibrium with the external loads

and lying within the structural domain (Como, 2013; Heyman, 1969; Huerta, 2006a, 2006b; Ochsendorf, 2002). Moreover, limit analysis is also a powerful method when the aim is to assess statically indeterminate structures and, thus, to explore the infinite set of admissible, internal stress states (Como, 2013). Many strategies apply such a theorem computationally to explore different equilibrium solutions. In particular, Fraternali *et al*. (2002), Angelillo and Fortunato (2004), Block *et al*. (2006a), Block and Ochsendorf (2007), Fraternali (2010); Block and Lachauer (2014); De Chiara *et al*. (2019); Gesualdo *et al*. (2019) D'Ayala and Casapulla (2001) and Mousavian and Casapulla (2020) modelled the structures as a continuum, whereas Livesley (1978, 1992), Gilbert *et al*. (2006), Orduña and Lourenço (2005), Portioli *et al*. (2014, 2015) and Gilbert and Melbourne (1994) modelled the structure as an assembly of rigid blocks having a finite friction capacity.

This paper focuses on the rigid-block equilibrium (RBE) method, which frames the equilibrium problem (EP) (Angelillo *et al*., 2018) as an optimisation problem that minimises the total amount of contact forces, having equilibrium relations and friction conditions as constraints. It is based on a formulation that was first proposed by Livesley (1978, 1992) and later extended by Whiting (2012) and Whiting *et al*. (2009) and Frick *et al*. (2015, 2016). Livesley proposed a mathematical model that adapts the analysis of rigid-plastic structural frames for finding the limit load of masonry structures formed by rigid blocks. In particular, the solution is obtained as the result of an optimisation problem, in which the load factor is maximised subject to the equilibrium linear constraints (Livesley, 1978). Later on, Livesley extended his previous study to three-dimensional (3D) masonry structures and uses an lower-bound approach to handle collapse mechanisms that involve sliding, hinging and twisting (Livesley, 1992). In his study, masonry structures are modelled as discrete elements that connect with rectangle planar interfaces and have a finite friction capacity – that is, assuming that the two surfaces in contact are slightly concave, and thus they interact through forces only at the corners. Whiting (2012) and Whiting *et al*. (2009) extended the method by including penalty forces to enlarge the solution space by allowing infeasible solutions to taking into account tension capacity on an interface as imaginary glue. Frick *et al*. (2015) reviewed the study of Whiting (2012) and proposed some visualisation methods to design discrete-element assemblies more intuitively. Frick *et al*. (2016) proposed a computational method that enables the possibility to calculate arbitrarily placed assembly with polygonal planar interfaces using a combined graph and mesh data structure.

This paper aims to review and develop the RBE method, and interpret its results by way of mathematical programming. The results of the virtual nodal forces were post-processed and reduced to their resultants on the contact interfaces to give them a structural meaning. Moreover, it was shown how RBE can be used to explore different internal stress states, allowing direct and easy control of the mechanical model. Compared with other commonly used tools, such as discrete-element modelling (DEM) – for example, using the 3DEC code (Cundall, 1971), RBE is open-source, fast, explicit and straightforward. It only needs one mechanical parameter (i.e. the friction angle, see also Iannuzzo *et al*., 2021). On the contrary, compared with real-time interactive environments such as physics-based game engine PhysX (Nvidia Physx Library, 2013) and Bullet (Bullet-Physics-Library, 2012), RBE provides more transparent and accurate results beyond a Yes/No answer – that is, stable or collapsing. RBE combines the rigour of both DEM and the interactivity speed of a game engine in order for it to be used for design purposes.

This research study explores and contributes to various aspects of the existing RBE formulation. First, the primal use of the kern is introduced, which for a unilateral material (i.e. rigid blocks in a unilateral contact) is the interface area in which a compressive point load may be applied without producing any tensile stress. Second, the mathematical formulation is revisited and the physical meaning of RBE results is discussed. Two different objective functions are compared, quadratic and linear, considering both nodal forces and interface resultants placed at the centres of pressure. Third, it is demonstrated that RBE can be used to explore various admissible stress solutions. Finally, RBE is related to practical masonry problems. First, two basic benchmarks are considered to show the main features of simple examples that can be checked manually. After that, examples, such as a semi-circular arch on buttresses and a hemispherical dome, are considered to demonstrate the potential of RBE.

2. Methodology: computational framework

In this section, the main features of RBE and how it is implemented computationally using the COMPAS framework are introduced (Van Mele *et al*., 2017). In particular, in Section 2.1, the main characteristics of the assembly data structure, which are used to handle complex geometrical data, are briefly recalled. In Section 2.2, the computational procedure adopted to define the kern of a polygonal section is introduced. In Section 2.3, the RBE method and its optimisation procedure, including the original quadratic formulation and the linear one used in the current paper, is introduced.

2.1 Rigid-block assembly data structure

Frick *et al*. (2016) presented a data management system to numerically model an arbitrarily placed assembly (Figure 1(a)) using a graph $G(V, E)$, where vertices V store

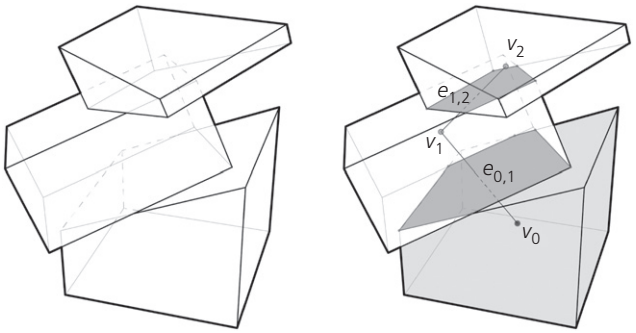

Figure 1. Arbitrarily placed rigid-block assembly (a) can be represented an assembly data structure through a graph $G(V, E)$ (b), where the nodes store block data and edges store contact data. The lower block, coloured in grey and denoted with v_0, is assumed as support (b)

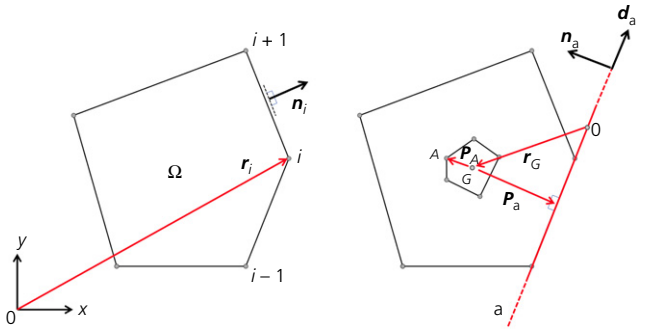

Figure 2. In (a), a convex, polygonal region Ω, whose generic vertex i is denoted through the vector $\boldsymbol{r}_i$ with respect to a generic reference system (O, x, y). In (b), the kern of the polygonal interface, and the correspondence among the tangent line a and its pole A

geometrical data of blocks and edges E store interface data that include geometrical and mechanical features (Figure 1(b)). Several interface typologies are available to model non-perfect contacts such as face–face, face–edge and face–vertex contacts.

For a complete description of the computational algorithm used to detect the interfaces and for a more detailed discussion of the assembly data structures, the reader is referred to Frick *et al.* (2016).

2.2 Kern of a generic polygonal interface

In this section, the numerical procedure adopted to define the kern of a generic and planar polygonal interface is illustrated, which can be either a convex or a concave interface (in the latter, the convex hull of the interface is used to define the kern). For more details, the reader is referred to Hally (1987) and Romano (2002). For unilateral materials, the kern of an interface is the area in which a compressive point load may be applied without producing any tensile stress. Looking at the n-vertex polygonal interface Ω (Figure 2(a)) defining a planar contact between two adjacent blocks, let $\boldsymbol{r}_i$ be the position vector of the ith vertex and $\boldsymbol{R}$ be the second-order, skew-symmetric tensor that rotates in the positive direction (right-hand rule) of any vector by $\pi/2$.

The unit outward normal $\boldsymbol{n}_i$ to the edge having length l_i and whose vertices are i and $i+1$ can be expressed as

$$\boldsymbol{n}_i = \frac{1}{l_i}\boldsymbol{R}(\boldsymbol{r}_{i+1} - \boldsymbol{r}_i) \tag{1}$$

The following three linear equations express the zero-, first- and second-order area moments, namely

$$A = \frac{1}{2}\int_{\partial\Omega} \boldsymbol{r}\cdot\boldsymbol{n}\,\mathrm{ds} = \frac{1}{2}\sum_{i=1}^{n} \boldsymbol{r}_{i+1}\cdot\boldsymbol{r}_i \tag{2}$$

$$\mathbf{S}_0 = \frac{1}{3}\int_{\partial\Omega} (\boldsymbol{r}\otimes\boldsymbol{r})\boldsymbol{n}\,\mathrm{ds} = \frac{1}{6}\sum_{i=1}^{n} \left(\boldsymbol{r}_{i+1}^{\perp}\cdot\boldsymbol{r}_i\right)(\boldsymbol{r}_{i+1}+\boldsymbol{r}_i) \tag{3}$$

$$\mathbf{J}_0 = \frac{1}{3}\int_{\partial\Omega} (\boldsymbol{r}\cdot\boldsymbol{n})\boldsymbol{r}\otimes\boldsymbol{r}\,\mathrm{ds} = \frac{1}{12}\sum_{i=1}^{n}\left(\boldsymbol{r}_{i+1}^{\perp}\cdot\boldsymbol{r}_i\right) \times\left(\boldsymbol{r}_i\otimes\boldsymbol{r}_i + \frac{1}{2}(\boldsymbol{r}_i\otimes\boldsymbol{r}_{i+1} + \boldsymbol{r}_{i+1}\otimes\boldsymbol{r}_i) + \boldsymbol{r}_{i+1}\otimes\boldsymbol{r}_{i+1}\right) \tag{4}$$

in which

$$\boldsymbol{r}_{i+1}^{\perp} = \frac{1}{l_i}\boldsymbol{R}(\boldsymbol{r}_{i+1} - \boldsymbol{r}_i) \tag{5}$$

Particularly, Equations 2–4 can be thought of as a scalar, a two-dimensional (2D) vector and a matrix, respectively. The position of the centroid of the interface $\boldsymbol{r}_G$ can be evaluated using Equations 2 and 3 as

$$\boldsymbol{r}_G = \mathbf{S}_0/A \tag{6}$$

and vertex A of the kern corresponding to line a (Figure 2(b)), as

$$7. \quad \boldsymbol{p}_A = -\mathbf{J}_G \boldsymbol{n}_a / A \boldsymbol{p}_a \cdot \boldsymbol{n}_a$$

By applying Equation 7 for each edge of the convex hull, it is possible to explicitly define the kern of a polygonal interface (Romano, 2002). In the next sections, how the kern of an interface can be introduced directly into RBE is shown. Furthermore, it is illustrated how, for statically indeterminate structures, it can be used to seek one of the infinite, admissible, internal stress fields that fully activate a set of interfaces.

Remark 1. Instead of adopting a *geometric safety factor* using the concept of 'kern' by shrinking the boundaries of the contact polygon (Whiting *et al*., 2009), the explicit kern formulation is implemented. The reason behind the use of the 'kern' in Whiting *et al*. (2009) was to prevent potential high concentrations of compressive stresses/forces just taking into account reduced interfaces. For a real material having a finite capacity in compression, high-level, localised compressive stresses can lead to material crushing. The main consequence of local material crushing is the redistribution of the compressive stresses over an augmented area, and the corresponding kinematic effects may be modelled in terms of relative displacements as a penetration between the original rigid blocks. Nonetheless, in common unreinforced, historic masonry structures, the effects of crushing on the stability are usually two orders of magnitude smaller than the common effects due to the typical crack pattern – for example, the ones caused by settlements. Therefore, it is very conservative to consider an assembly with reduced interfaces. It is more reasonable to take into account these secondary effects in the post-processing phase unless the adopted model allows accounting for plastic compressive deformations directly. For a rigid-block model with a finite compressive capacity, the reader is referred to Portioli *et al*. (2015).

2.3 Rigid-block equilibrium (RBE) method

In this section, it is briefly illustrated how RBE frames and solves the EP as an optimisation problem. After introducing the original quadratic formulation (Whiting, 2012; Whiting *et al*., 2009), a linear formulation is presented, which will be used in the following applications to explain some key features of the RBE approach.

An *assembly* composed of convex blocks, arbitrarily placed and with a potential of imperfections is considered. Figure 3 illustrates the main characteristics of the assembly data structure once the graph is constructed and all the corresponding interfaces, along with their geometrical characteristics, are identified.

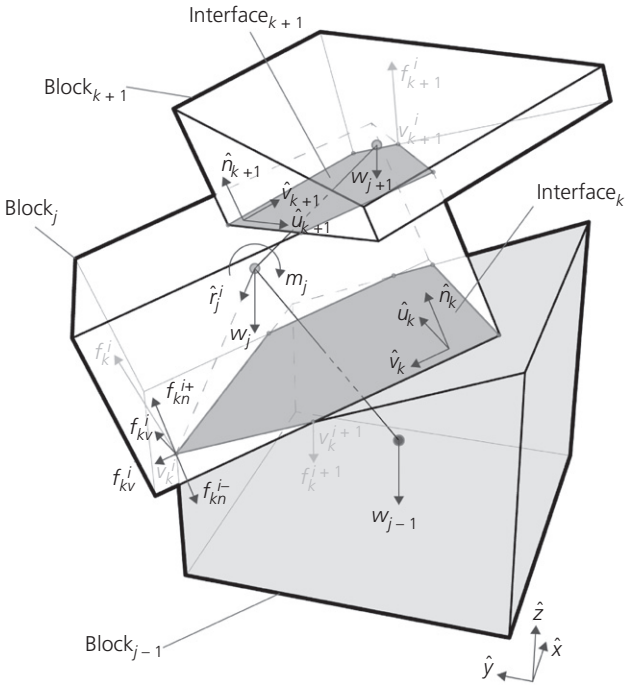

Figure 3. 3D view of an assembly of randomly placed blocks. Block$_{j-1}$ is support, whereas the remaining are free blocks. $(\hat{\boldsymbol{n}}_k, \hat{\boldsymbol{u}}_k, \hat{\boldsymbol{v}}_k)$ is the local reference system of each l_k-sided polygonal interface. The external forces are reduced to their resultants and torques acting on the centroid of each block. The nodal forces are represented as vectors in the $(\hat{\boldsymbol{n}}_k, \hat{\boldsymbol{u}}_k, \hat{\boldsymbol{v}}_k)$ reference system: $\boldsymbol{f}^i_{ku} = f^i_{ku}\hat{\boldsymbol{u}}_k$, $\boldsymbol{f}^i_{kv} = f^i_{kv}\hat{\boldsymbol{v}}_k$, $\boldsymbol{f}^{i+}_{kn} = f^{i+}_{kn}\hat{\boldsymbol{n}}_k$, and $\boldsymbol{f}^{i-}_{kn} = -f^{i-}_{kn}\hat{\boldsymbol{n}}_k$, with f^i_{ku}, $f^i_{kv} \in \mathbb{R}$ and f^{i+}_{kn}, $f^{i-}_{kn} \in \mathbb{R}^+_0$

The blocks of an assembly can be distinguished as supports (Block$_{j-1}$ in Figure 3) or free blocks (the remaining ones). Since RBE is based on a concave contact formulation (Livesley, 1992), the interaction between two adjacent blocks is modelled through forces acting on the vertices of an interface. The Interface$_k$ is an l_k-sided polygon (l_k being the number of its vertices) and its local reference system is denoted with $(\hat{\boldsymbol{n}}_k, \hat{\boldsymbol{u}}_k, \hat{\boldsymbol{v}}_k)$, in which $\hat{\boldsymbol{n}}_k$ is the normal unit vector and $\hat{\boldsymbol{u}}_k$ and $\hat{\boldsymbol{v}}_k$ are two arbitrary, mutually orthogonal and in-plane unit vectors. A generic vertex of Interface$_k$ is $\boldsymbol{v}^i_k \in \mathbb{R}^3$ with $i \in \{1, \ldots, l_k\}$, whereas the corresponding contact force $\boldsymbol{f}^i_k \in \mathbb{R}^3$ is a 3D vector having one normal and two tangential components.

2.3.1 Equilibrium

The static equilibrium of the entire assembly can be generalised and formulated in the matrix form

$$8. \quad \mathbf{A}_{eq}\boldsymbol{f} = -\boldsymbol{p}$$

where $\mathbf{A}_{eq}$ is the equilibrium matrix, $\boldsymbol{f}$ consists of all internal forces and $\mathbf{p}$ is the vector collecting the external forces – that is, the net forces $\mathbf{w}$ and torques $\mathbf{m}$ acting on the centroids of the blocks.

Let g be the number of blocks and h the number of the interfaces, relation (8) can be expressed as

$$9. \quad \begin{bmatrix} \mathbf{A}_{0,0} & \cdots & \mathbf{A}_{0,h} \\ \vdots & \ddots & \vdots \\ \mathbf{A}_{g,0} & \cdots & \mathbf{A}_{g,h} \end{bmatrix} \begin{bmatrix} \boldsymbol{f}_0 \\ \vdots \\ \boldsymbol{f}_h \end{bmatrix} = - \begin{bmatrix} \boldsymbol{p}_0 \\ \vdots \\ \boldsymbol{p}_g \end{bmatrix}$$

where $\mathbf{A}_{j,k}$ represents the equilibrium matrix for the Block$_j$ with respect to the Interface$_k$; $\mathbf{f}_k$ is the vector collecting all nodal forces on the l_k-sided polygonal Interface$_k$; $\boldsymbol{p}_j \in \mathbb{R}^6$ are the external forces acting on Block$_j$ and, $\boldsymbol{p}_j$ consists of translation self-weight $\mathbf{w}_j \in \mathbb{R}^3$ and rotational torque $\mathbf{m}_j \in \mathbb{R}^3$ parts. In particular, the jth row of Equation 9 represents the equilibrium of Block$_j$. Specifically, it is written as taking into account all interface forces concerning all blocks of the assembly connected with Block$_j$.

The forces on the Interface$_k$ acting on Block$_j$ can be represented in a matrix form as

$$10. \quad \mathbf{A}_{j,k} \cdot \boldsymbol{f}_k = \begin{bmatrix} \mathbf{a}_{kx} & \mathbf{a}_{kx} & \cdots & \mathbf{a}_{kx} \\ \mathbf{a}_{ky} & \mathbf{a}_{ky} & \cdots & \mathbf{a}_{ky} \\ \mathbf{a}_{kz} & \mathbf{a}_{kz} & \cdots & \mathbf{a}_{kz} \\ \mathbf{b}^i_{j,kx} & \mathbf{b}^{i+1}_{j,kx} & \cdots & \mathbf{b}^{i+l}_{j,kx} \\ \mathbf{b}^i_{j,ky} & \mathbf{b}^{i+1}_{j,ky} & \cdots & \mathbf{b}^{i+l}_{j,ky} \\ \mathbf{b}^i_{j,kz} & \mathbf{b}^{i+1}_{j,kz} & \cdots & \mathbf{b}^{i+l}_{j,kz} \end{bmatrix} \begin{bmatrix} \boldsymbol{f}^i_k \\ \boldsymbol{f}^{i+1}_k \\ \vdots \\ \boldsymbol{f}^{i+l}_k \end{bmatrix}$$

where $\mathbf{a}_{kx} = [\,\hat{n}_{kx} \quad \hat{u}_{kx} \quad \hat{v}_{kx}\,]$, $\mathbf{b}^i_{j,kx} = \left[\, \left(\boldsymbol{r}^i_j \times \hat{\boldsymbol{n}}_k\right)_x \quad \left(\boldsymbol{r}^i_j \times \hat{\boldsymbol{u}}_k\right)_x \quad \left(\boldsymbol{r}^i_j \times \hat{\boldsymbol{v}}_k\right)_x \,\right]$ and $\boldsymbol{f}^i_k = [\, f^i_{kn} \quad f^i_{ku} \quad f^i_{kv}\,]^{\mathrm{T}}$, where the torque arm $\boldsymbol{r}^i_j$ can be expressed as $\left|\boldsymbol{r}^i_j\right| \hat{\boldsymbol{r}}^i_j$, with $\hat{\boldsymbol{r}}^i_j$ being the related unit vector (Figure 3). It is worth noting that $\boldsymbol{f}^i_k$ collects the three scalar components of the nodal forces with respect to the local axes of the interface.

2.3.2 Penalty formulation and lower-bound values

Whiting *et al.* (2009) and Whiting (2012) introduced a penalty formulation that decoupled the normal components f^i_{kn} of the nodal forces $\boldsymbol{f}^i_k$ as

$$11. \quad f^i_{kn} = f^{i+}_{kn} - f^{i-}_{kn}$$

with $f^{i+}_{kn}, f^{i-}_{kn} \in \mathbb{R}^+_0$ the positive and the negative parts of f^i_{kn}, respectively.

2.3.3 Friction constraints

For a rigid-block assembly, the Mohr–Coulomb yield criterion is commonly adopted to simulate the unilateral interaction among the blocks to take into account the sliding phenomena. It is represented by a conic yield surface. RBE takes into account this aspect through an eight-sided cone constraint to linearly approximate the conic surface. Specifically, the friction constraint is enforced in the matrix form in terms of $\boldsymbol{f}^i_k$ as

$$12. \quad \mathbf{A}_{fr}\boldsymbol{f} \leq \mathbf{0}$$

For more details, the reader is referred to Livesley (1992), Whiting *et al.* (2009) and Frick *et al.* (2015). Since RBE is based on a penalty formulation, two strategies can be adopted to model the friction constraint through Equation 12. The first relates the tangential forces with the net normal forces (Whiting, 2012; Whiting *et al.*, 2009), namely

$$13. \quad \left|f^i_{kt}\right| \leq \mu \left(f^{i+}_{kn} - f^{i-}_{kn}\right)$$

the second relates the tangential forces only with the positive part of the normal forces (Frick *et al.*, 2015) – that is

$$14. \quad \left|f^i_{kt}\right| \leq \mu f^{i+}_{kn}$$

where μ is the static friction coefficient. The first strategy is called *friction-net* approach, whereas the second *friction+* approach. With the *friction-net* approach, the optimisation problem can get infeasible if the friction capacity is overcome. Indeed, if the net force of Equation 13 is zero, the corresponding tangential force is constrained to be zero. With the *friction+* approach, the problem is always feasible since the solution in terms of tangential forces affects the normal nodal forces due to the penalty formulation. In Section 3.1.2, this aspect is illustrated through a simple benchmark.

It is pointed out that the friction constraint Equation 12 is defined on the interface nodes. In this sense, the friction value used is a *local friction coefficient*. In what follows, the friction capacity of an interface is post-processed as a *global friction capacity* – that is, in terms of normal and tangential interface resultants, to better understand the physical behaviour. This does not affect the results, as if the friction constraint is fulfilled locally (i.e. on interface corners), namely

$$15. \quad \left|f^i_{kt}\right| \leq \mu\left(f^{i+}_{kn}\right), \quad \forall i \in \{1, \ldots, l_k\}$$

then, it is even globally satisfied (whole interface) – that is,

$$16. \quad \sum_{i}^{k} |f_{kt}^{i}| \leq \mu \sum_{i}^{k} f_{kn}^{i+}$$

To also overcome potential infeasibility states due to the *friction-net* approach, one can adopt a local friction value to be used in the optimisation and define a threshold to detect if the global friction capacity of an interface is overcome or not. In the opinion of the authors, this last approach is consistent with the RBE objective function since by also penalising the friction forces, the method provides an equilibrium solution with the smallest amount of tangential forces. In Section 3.1.2, the main differences between these two strategies are illustrated, but the *friction-net* approach is used in all remaining applications.

2.3.4 Equilibrium as an optimisation problem

Once the equilibrium and friction constraints are introduced, the equilibrium is solved as an energy-minimisation problem, namely

$$\boldsymbol{f}_{\mathrm{QP}}^{*} = \underset{\boldsymbol{f}}{\operatorname{argmin}} \frac{1}{2} \boldsymbol{f}^{\mathrm{T}} \mathbf{H} \boldsymbol{f}$$

$$\text{s.t. } \mathbf{A}_{\mathrm{eq}} \mathbf{f} = -\mathbf{p}$$

$$\mathbf{A}_{\mathrm{fr}} \boldsymbol{f} \leq \mathbf{0}$$

$$17. \quad \mathbf{I}_{\mathrm{lb}} \boldsymbol{f} \geq \mathbf{0}$$

where $\mathbf{H} = \mathrm{diag}(\boldsymbol{c})$ is a diagonal matrix and the entries of the vector $\boldsymbol{c}$ are the weights attributed to the compressive, tensile and friction forces (Whiting, 2012). To show the main features of RBE and to illustrate some key points of a limit analysis-based approach, the results of the optimisation problem 17 are used and compared with the ones obtained using the same constraints, but assuming a linear objective function – that is,

$$18. \quad \boldsymbol{f}_{\mathrm{LP}}^{*} = \underset{\boldsymbol{f}}{\operatorname{argmin}} \ \boldsymbol{c}^{\mathrm{T}} \boldsymbol{f}$$

Problem 17 is a quadratic optimisation problem (QP) so it will be referred to as the QP, whereas problem 18 is a linear-programming problem indicated with linear optimisation problem (LP). The solution of both the optimisation problems returns nodal forces needed for the static equilibrium of the assembly with the smallest amount of compressive, tensile (highly penalised) and friction forces.

In the next analysis, to verify the results, all nodal forces acting on an interface will be reduced to their resultants (forces and torques if present) applied at the centre of the pressure of the interface. Moreover, compressive nodal forces are plotted in blue, tensile forces in red, interface resultants in dark green and interface torques in black. However, in all of the examples in the paper, torques are negligible and, thus, too small to be recognised.

It is worth noting that the penalty formulation only regards the normal contact forces. Thus, infeasible-equilibrated solutions can be explored, even when the actual friction value is overcome by adopting a high-friction coefficient and defining a friction threshold in the post-processing phase to check if the friction capacity of an interface is overcome (red interfaces) or not (yellow interfaces). This approach is consistent with the definition of the objective function of the optimisation problems since it allows finding equilibrated solutions with the smallest amount of friction forces also. From the computational point of view, both QP and LP optimisation problems will be solved with CVXPY (Diamond and Boyd, 2016) using IBM CPLEX (CPLEX II, 2009) as a solver.

3. Applications

In this section, to illustrate, compare and interpret the RBE results, three main examples are considered that have an increasing complexity, thus an increasing static indeterminacy: an assembly of two stacked blocks, a buttressed arch and a dome. In all cases, both optimisation problems are adopted to clarify the main differences between two approaches: QP and LP. Additionally, it will be shown how to explore/select different internal stress states on the reference configuration and how to define the limit state for increasing horizontal loads.

3.1 Two stacked blocks

In this section, simple assemblies composed of two stacked blocks are considered, to illustrate some features of RBE. For all examples, only the self-weight is considered as an external force. The first analysis (Section 3.1.1) illustrates the rule of the normal contact forces by considering two blocks having a horizontal interface in different scenarios obtained by horizontally translating the upper block. With the second analysis (Section 3.2), the role of the tangential contact forces is shown, illustrating how the friction capacity can be taken into account

using both friction strategies. In all cases, the analyses are solved and compared using both the original quadratic formulation (QP) and the linear one (LP).

3.1.1 Horizontal interface

In this section, an assembly composed of two vertically stacked blocks with a horizontal contact interface is considered. The upper block, whose centroid is denoted with a blue dot, is a free block, whereas the bottom block, denoted with a red dot, is assumed to be a support. Figure 4 shows the first RBE analysis considering a fully connected interface. The solution of both QP (Figure 4(a)) and LP (Figure 4(b)) returns nodal forces that are vertical only. As one can notice, the distribution of the nodal forces obtained through the QP is different from the one obtained through the LP. In this case, the different nodal force distributions over an interface are highlighted by using a colour gradient.

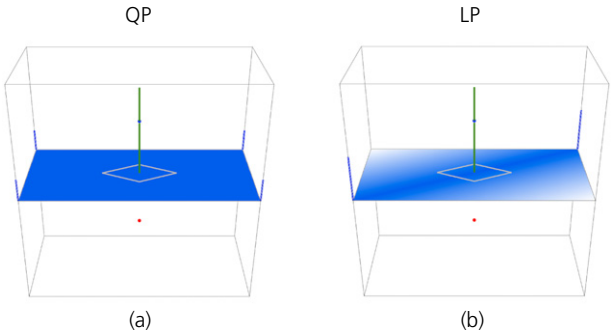

Figure 4. Two blocks stacked vertically with a horizontal contact interface: nodal forces and resultants from QP (a) and LP (b) formulations. The interfaces are depicted using a blue colour gradient to differentiate different nodal-force distributions. Resultants (in green) from both QP (a) and LP (b) formulation are the same

Nonetheless, if the nodal forces are reduced to their resultants (in green), one can observe that the same solutions are obtained. These solutions are trivially in equilibrium being the resultants going through the centre of mass of the upper blocks.

If the upper block is horizontally translated, as shown in Figure 5, a different distribution of the normal contact forces is always obtained from QP and LP. However, the resultants are still the same.

This observation can also be noted in the last analyses (Figures 5(c) and 5(f)) where the vertical projection of the centre of mass of the upper block is lying outside the interface; the tensile nodal forces appear due to the penalty formulation expressed by Equation 11. This last result represents a key feature of the RBE approach. Despite other equilibrium approaches adopted in the limit analysis framework, RBE goes beyond the Yes/No answer coming from the *feasibility/infeasibility* of an optimisation problem. Indeed, RBE allows non-stable solutions to be described and, thus interfaces subjected to tensile forces to be localised. In this sense, the penalty formulation enlarges the space of admissible stress fields.

3.1.2 Inclined interface

In this section, to clarify the main features of both *friction-net* and *friction+*, an assembly composed of two vertically stacked

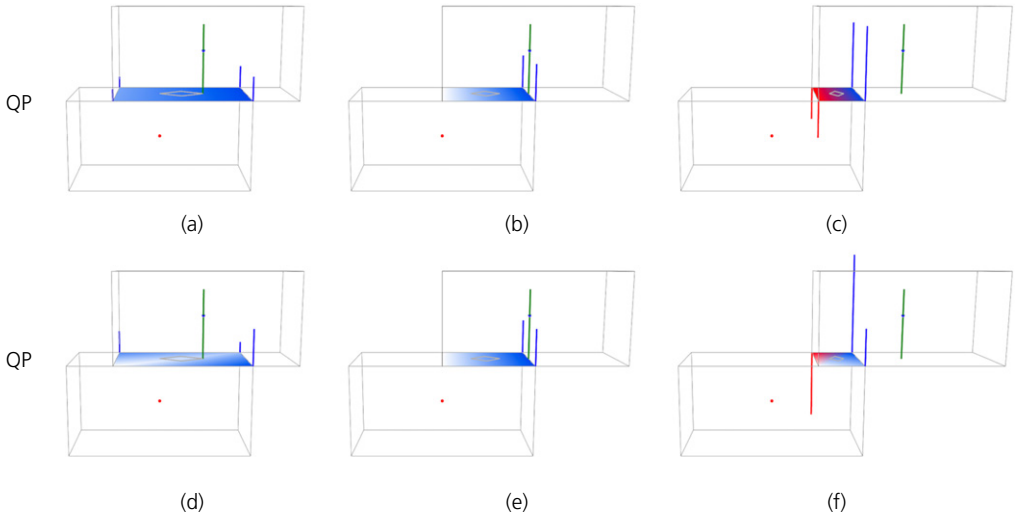

Figure 5. Equilibrium results from the RBE when the upper free block is horizontally translated, both QP (a, b, c) and LP (d, e, f). The problem is still feasible even when the upper block is in a non-stable condition (c, f)

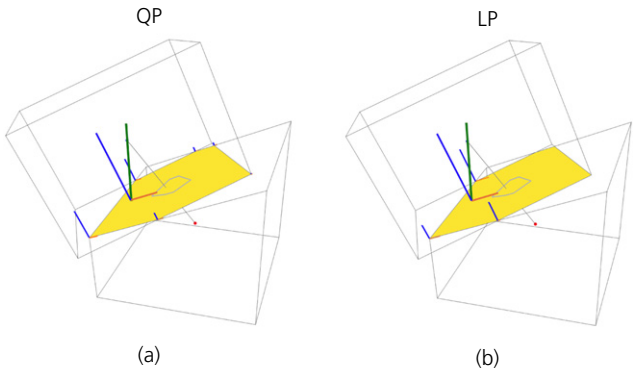

Figure 6. Solution of the QP (a) and LP (b) optimisation problems with the *Friction-net* approach. Two blocks stacked vertically with an inclined interface (25°). The friction coefficient is equal to 0.8 and the threshold is set to 0.6: the interfaces are depicted in yellow, meaning that the friction capacity is not overcome

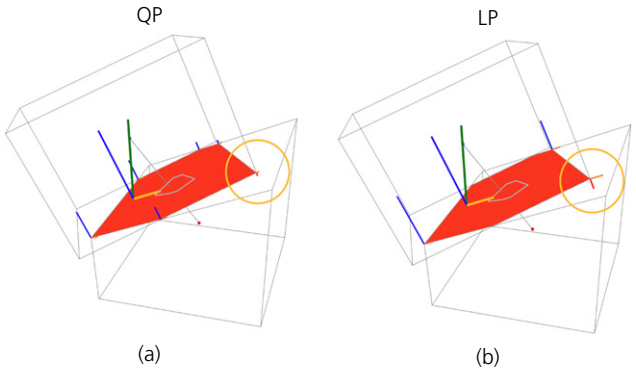

Figure 7. Solution of the QP (a) and LP (b) optimisation problems with the *Friction+* approach. Two blocks stacked vertically but with an inclined interface (23.6°). The friction coefficient here is assumed equals to 0.2. The interfaces are depicted in red, meaning that the friction capacity is overcome

blocks having an inclined interface is considered. The inclination of the interface is 23.6°, so the minimum friction value needed to guarantee the static equilibrium of the assembly is 0.44. The results are visualised in terms of nodal contact forces, normal and tangential resultant forces and global resultants (in green).

Figure 6 exhibits the RBE results using the *friction-net* approach. Specifically, a friction value equal to 0.8 and 0.6 is assumed as a threshold for evaluating the friction capacity. In this case, the interfaces are depicted in yellow since the global friction capacity is not overcome. If a smaller threshold is chosen (say 0.2) such that the friction capacity is overcome, the solution (in terms of both nodal forces and resultants) is trivially the same, but the interface would appear in red. The use of the *friction+* approach does not change the results if properly coupled with a threshold value. Conversely, if the local friction value is set as 0.2, with the *friction-net* approach, the problem becomes infeasible as the friction constraints (Equation 13) are not satisfied anymore. On the contrary, using the *friction+* approach, the problem is still feasible since, as shown in Figure 7, the tangential forces affect the solution of normal forces due to the penalty formulation.

Indeed, Figure 7 shows the RBE results using the *friction+* approach and a local friction coefficient equal to 0.2. As one can observe, with both QP and LP approaches (more evident in the second case), RBE finds a tensile tangential force in a corner (orange circle in Figure 7). In particular, referring to (Equation 14), at that corner, RBE finds both a non-zero positive (f_{kn}^{i+}) and negative (f_{kn}^{i-}) part, which results in a negative normal component f_{kn}^{i} (tensile force) being $f_{kn}^{i+} < f_{kn}^{i-}$. In this sense, the friction constraint, written as a function of the positive part, is still satisfied.

Remark 2. It is worth to mention that when no tensile force appears (i.e. f_{kn}^{i-} is zero), Equations 13 and 14 become identical; hence, *friction+* and *friction-net* provide the same solution.

3.1.3 Discussion

By looking at the nodal force distributions, in all cases, the LP solution is different from the QP. In particular, the QP approach tends to activate all nodes selecting solutions whose nodal forces have to be distributed as smooth as possible. Moreover, although every solution obtained with the QP approach can be a solution to the LP, the contrary may not happen. Indeed, the value of the QP objective function in the case of Figure 4(b) is greater than the one assumed for the solution depicted in Figure 4(a), while the LP objective function provides the same value for both solutions. For this reason, it is easy to observe that the solution space of LP is larger compared with that of QP.

The QP approach selects a nodal force distribution that comes from an elastic interpretation of the EP (Angelillo *et al.*, 2010). The LP formulation considers the interface as rigid and then infinite admissible stress states are possible (Iannuzzo *et al.*, 2020). From a limit analysis point of view, there is no reason to prefer one over another, since both represent admissible solutions. Furthermore, in terms of interface resultants, both are the same since the problem is statically determined.

In the second benchmark, two blocks with an inclined interface are analysed to illustrate the main differences between *friction-net* (Equation 13) and *friction+* (Equation 14) approaches that are solved using QP and LP (Figure 7). Both are valid strategies, particularly when coupled with a threshold to evaluate global friction capacity. The main difference is that, when

the local friction value is overcome, the problem is infeasible with the *friction-net* approach, whereas with the *friction+* approach it is still feasible but the normal force distribution is affected by the tangential behaviour due to the penalty formulation. In this sense, the *friction+* approach seems more in-line with the aim of RBE. Physically, it can be imagined that the *friction+* approach activates a tensile capacity (as a glue) that also provides a shear strength. Nonetheless, for many masonry problems, the *friction-net* approach is more useful when the aim is to explore the feasibility of the problem to catch ultimate equilibrium states. For this reason, in what follows, the *friction-net* strategy is adopted, assuming the friction coefficient to be 0.8 and the friction threshold to be 0.6.

3.2 Semi-circular arch on buttresses

In this section, a semi-circular arch on buttresses is considered to illustrate how RBE can be applied to assess unreinforced masonry structures. The geometry of the buttressed arch is the same used in Iannuzzo *et al.* (2020) where it was analysed to show the peculiarities of the piecewise rigid displacement (PRD) method, an energy-based limit analysis approach (Iannuzzo, 2019; Iannuzzo *et al.*, 2018). The semi-circular arch has an internal radius of 1.00 m, a thickness of 0.30 m, an orthogonal depth of 0.50 m and is discretised into 15 voussoirs. The two buttresses have a height of 2.5 m, a base of 0.70 m and a depth of 1.00 m and are partitioned into 12 elements. The two bottom blocks of the buttresses are considered as supports. The structure has a uniformly distributed mass density $\rho = 1800\,\mathrm{kg/m^3}$, and 0.6 is assumed as the friction threshold. In Section 3.2.1, the initial geometry is analysed. In Section 3.2.2, how to explore different equilibrated solutions is shown, whereas in Section 3.2.3, a tilting test of the structure is performed.

3.2.1 Initial configuration: LP against QP solutions

The first analysis considers the buttressed arch in its initial configuration. Figure 8 shows the solutions obtained by solving the QP and LP, respectively. As in the previous examples, the nodal force distributions, highlighted by the blue colour gradient, are different. However, although the two stacked blocks of Section 3 can admit only one equilibrated solution in terms of interface resultants, as the buttressed arch is statically indeterminate, the interface resultants are not the same, even if almost identical. Indeed, both QP and LP return solutions close to the minimum thrust. Moreover, as one can observe, thrusts in the buttresses are everywhere within the kern, meaning that all buttress interfaces are activated fully in compression.

3.2.2 Explore different admissible-equilibrated stress states

In this section, a procedure is illustrated that can be used to explore different admissible, singular, internal, stress states. The idea is to consider new virtual interfaces, which can be

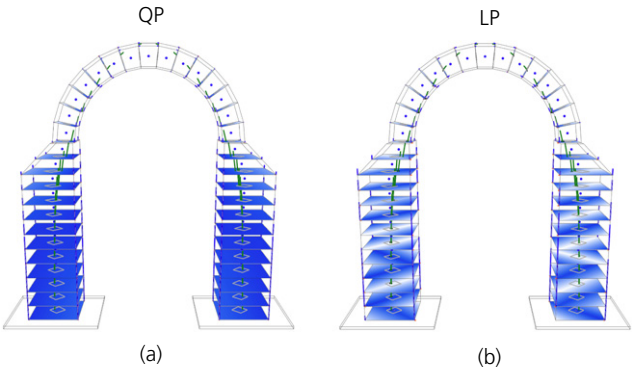

Figure 8. A buttressed arch in its initial reference configuration: both QP (a) and LP (b) solutions return a thrust line that is linked to a minimum thrust condition of the semi-circular arch. The interface resultants in the buttresses are everywhere within the corresponding interface kern

obtained by tightening the original interface and writing the equilibrium Equation 8 on these new (reduced) interfaces. Following this approach, a thrust line solving the EP is considered, that either crosses or is as close as possible to the new, reduced interfaces. A similar procedure was adopted by Iannuzzo *et al.* (2020) using the PRD method. Although, in Iannuzzo *et al.* (2020) only a precise Yes/No answer could be obtained, with the RBE approach and its penalty formulation a solution can also be selected that does not fit the prescribed requirement completely. In this case, tensile forces on the nodes of the reduced interfaces can appear, meaning that the thrust line cannot be contained within the reduced interfaces.

In Figures 9(a) and 9(c), the key-stone interface is tightened to explore a maximum thrust condition for the semi-circular arch, which leads the buttresses under the worst working conditions, being the interface resultants outside the kern at the bases of the buttresses. Figures 9(b) and 9(d) show the results obtained by enforcing the thrust line to go through the kern of all interfaces of the arch (*kern-fitting*). Both the QP and LP return almost identical interface resultants, thus only the resultant forces are visualised.

Moreover, using the *friction-net* approach, it can be possible to select an internal stress state that also fulfils particular requirements of the friction capacity. Indeed, if a low value for the friction coefficient is chosen (thus, without adopting a threshold strategy), the problem can become infeasible. The lowest value of the friction angle for which the problem is still feasible represents the minimum friction value required by the assembly to be in static equilibrium. In this case, the minimum value is found to be 0.31. In Figure 10(a), the solutions for the corresponding EPs are depicted both in terms of nodal forces

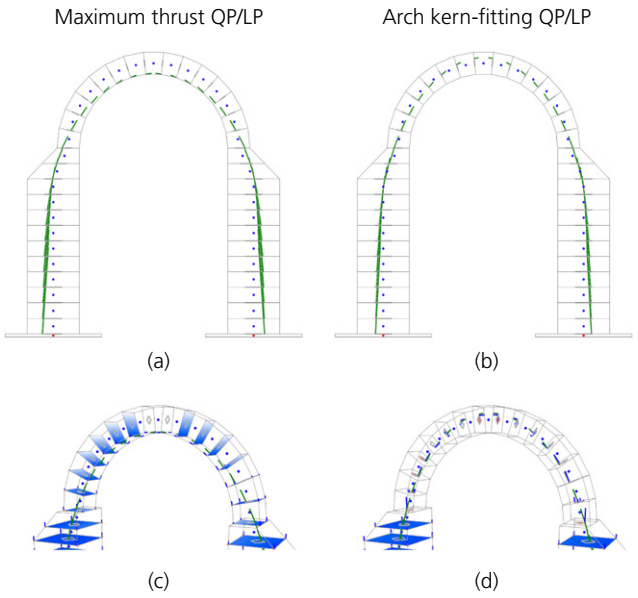

Figure 9. In (a), the mid-span interface of the semi-circular arch is reduced as highlighted in (c) to select an admissible internal stress state for which the thrusts exerted on the buttresses are maximised. The same solution can be obtained by reducing the two base-interfaces of the arch (towards the extrados). In (b), the interfaces of the semi-circular arch are virtually reduced to their kerns as highlighted in (d) to seek if there is a thrust line that fully activates the arch in compression. As one can observe, the thrust is outside the mid-span interface. For both examples, the results of the QP and LP are almost identical, so the resultant can only be visualised in (a) and (b)

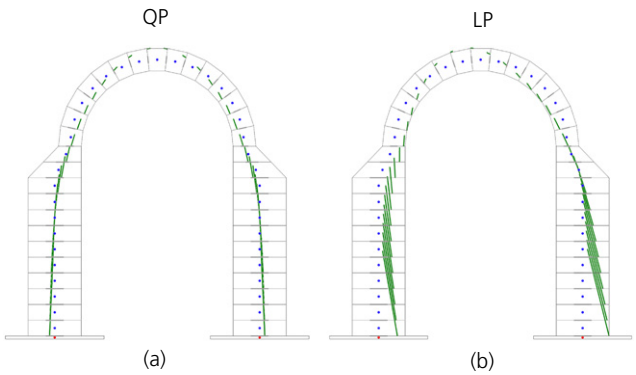

Figure 10. In (a), using the *friction-net* approach, RBE returns 0.31 as the lowest value of the friction coefficient for which the assembly is still in equilibrium. The resultants are everywhere in the friction cone. In (b), the buttressed arch subjected to a tilting test: the maximum angle for which the resultants are everywhere within the structural geometry is 12°

and resultants. It can be noted that the resultants are everywhere within the reduced friction cone.

3.2.3 Tilting test: horizontal external forces

A common way adopted for considering the stability of masonry structures when subjected to horizontal static forces is to perform a tilting test (Block *et al.*, 2006b). This scenario is modelled by rotating the gravity vector until tensile forces appear. The maximum value of the tilting angle for which the thrust line is everywhere within the structural domain is 12°, which corresponds to a horizontal static multiplier of 0.21, which is very close to the one found in Iannuzzo *et al.* (2020). In Figure 10(b), the solutions are depicted: it touches the structural boundary in four points, three on the arch and one at the base on the right. These four points suggest a mechanism that is the same as that found in Iannuzzo *et al.* (2020), as the PRD approach allows also evaluating mechanisms due to seismic forces.

3.2.4 Discussion

In this section, considering a buttressed arch, some RBE analyses are performed using both QP and LP approaches: assessing the initial configuration; exploring various internal equilibria; finding the minimum friction and evaluating the maximum horizontal static multiplier for which the assembly is still in equilibrium. All analyses show that solving the QP and LP, different nodal forces can be obtained, confirming the discussion in Section 3.1. Despite the case of stacked blocks, which is globally (in terms of interface resultants) statically determined, the buttressed arch is globally statically indeterminate, and, for this reason, when the initial configuration is considered, the QP and LP solutions, in terms of resultants, are slightly different. Nonetheless, the QP and LP solutions are the same when approaching a limit state (e.g. tilting test), since the solution is unique and using the *friction-net* approach is dictated by the feasibility of the problem. In the next section, how an increase in the global indeterminacy of the system can increase the differences between QP and LP is shown. Nonetheless, it is pointed out that in any case, solutions coming from both the optimisations represent two statically admissible stress fields, and in this sense, safe solutions matching the spirit of the safe theorem.

3.3 Hemispherical dome

In this section, a hemispherical dome is considered with an oculus to illustrate how to apply RBE to assess 3D-unreinforced masonry structures. The centre-line radius R of the dome is 5 m whereas the thickness t is assumed to linearly vary from the bottom base (0.50 m) to the top part (0.25 m). The radius r of the oculus is 1 m.

The dome is discretised using 14 meridian slices and 10 in parallels; therefore, the number of blocks is 140. The blocks of the bottom ring are assumed as supports (Figure 11). The structural complexity of the dome is larger than the one of the

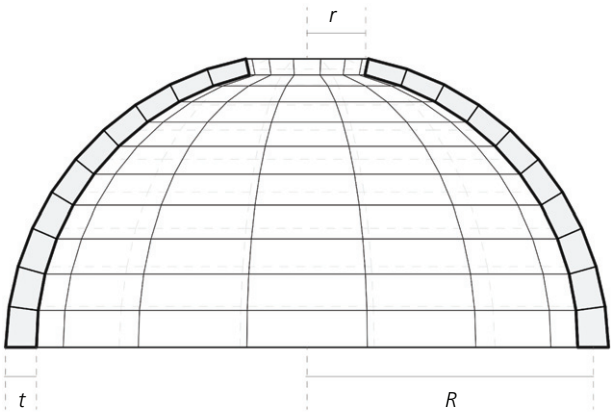

Figure 11. Cross-section and discretisation of the hemispherical dome: main dimensions. The mean radius R is 5 m; the radius of the oculus r is 1 m and the thickness t is assumed to linearly vary from 0.5 m (base) to 0.25 m (oculus)

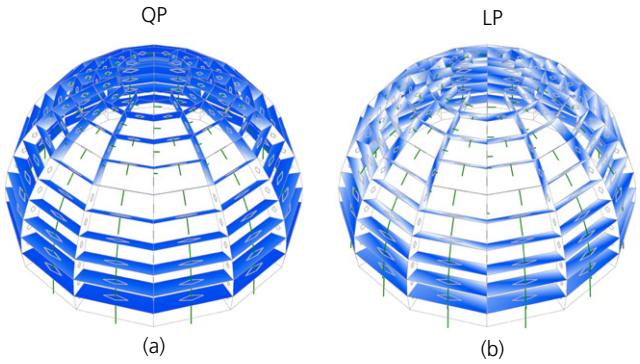

Figure 12. RBE analysis of the reference configuration: QP (a) and LP (b) solutions. The interface colour-distribution shows that these two solutions are locally different. Moreover, also the interface resultants are different, being the QP solution radial-symmetric. The white interfaces denote zero hoop-force regions

buttressed arch since, in the present case, the graph $G(V, E)$ describing the data structure is 2D. In Section 3.3.1, the initial geometry is analysed using both QP and LP. In Section 3.3.2, different equilibrium solutions are explored, including kern-fitting and *inner/outer base-fitting* analysis. In Section 3.3.3, the dome subjected to horizontal action is assessed and the maximum value of the horizontal multiplier is defined.

3.3.1 Initial configuration: LP against QP solutions

In this section, an RBE analysis of the reference configuration is proposed, without considering any further constraint. Figures 12(a) and 12(b) show results from QP and LP optimisations. The interfaces are still coloured using a blue-gradient colour map. However, the white interfaces denote the sections without any nodal force, or with forces less than a threshold value fixed at 10^{-2} of the maximum compressive force. Even though RBE can provide stress solutions with tensile forces, it returns a purely compressive internal stress state for which part of the meridian interfaces are affected by zero hoop forces (Heyman, 1997). Nonetheless, QP and LP solutions show different nodal force distributions that illustrate how the difference in terms of interface resultants is more evident in the present case than that in the previous ones. This aspect reflects on the extension (from the base) of the non-zero hoop-forces area (Figure 12). Moreover, the QP resultant is radial symmetric whereas the one from LP is not.

3.3.2 Exploring different equilibrium states

In this section, different internal stress states are explored. The first analysis is what is called a kern-fitting analysis – that is, an internal admissible stress field is considered, that everywhere is within the kern of all interfaces. The kern-fitting analysis coupled with the next inner/outer base-fitting analysis can provide a measure of the stability of the dome under its self-weight, and whose results can be related to the *geometric safety factor* (Huerta, 2006b). In Figures 13(a) and 13(b), the results of a kern-fitting RBE analysis are depicted: the interfaces are virtually reduced to their kern to seek if there is an internal stress field that fully activates all contacts. Figures 13 (c)–13(f) show the results of two analyses aimed at exploring admissible stress fields that are as much as possible close to the outer and inner parts of the supports, respectively. These results are obtained by virtually shrinking the bottom interfaces towards either the outer or the inner surface.

3.3.3 Tilting test: horizontal external forces

As for the buttressed arch, a tilting test is performed to explore the maximum allowable capacity of the dome subjected to horizontal actions. The maximum tilting angle found with RBE and both LP and QP analyses is 32°. Figure 14 shows the flow of the resultants within the structure. Despite the previous case, this RBE analysis is stopped because, using the friction-net approach, the problem becomes infeasible before tensile stresses appear (0.6 is adopted as the local friction value, to be consistent with the threshold value used in all analyses).

3.3.4 Discussion

In this section, looking at a dome with an oculus, different equilibrium solutions on the reference configuration are explored checking also its maximum capacity under increasing horizontal static actions. First, looking at the RBE analyses proposed in Sections 3.3.1 and 3.3.2, it is worth noting that even though RBE is based on a penalty formulation, which allows tensile forces, it always returns (when admissible) solutions having part of the meridian interfaces affected by zero hoop forces. Second, the

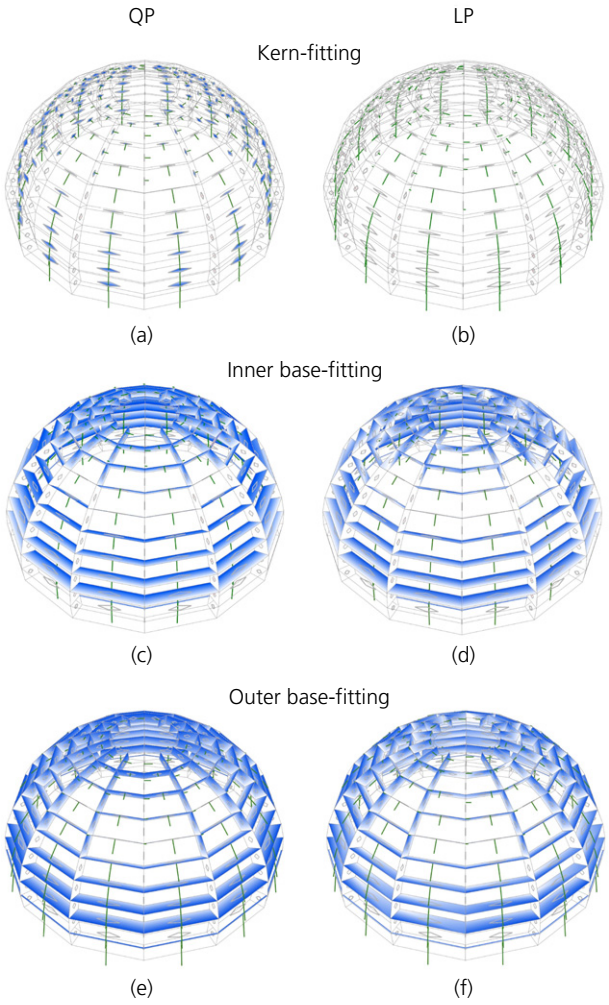

Figure 13. In (a, b), the results of the kern-fitting RBE analysis: QP (a) and LP (b) solutions. The interface resultants are enforced to go through all interface kerns. In (c, d), the resultants are enforced to go through the inner part of the support: QP (c) and LP (d) solutions. In (e, f), the resultants are enforced to go through the outer part of the support: QP (e) and LP (f) solutions. In all cases, QP and LP return two solutions that are very similar, particularly if one looks at the non-zero hoop-force areas

structural complexity of a dome is higher than the one of a buttressed arch, being the network of the graph $G(V, E)$ bi-dimensional. From this aspect, the hemispherical dome reflects into a larger statically indeterminate problem, which also affects the output of the QP and LP analyses, showing larger differences if compared with the buttressed arch. It has been shown how RBE can be used to explore different singular, internal stress states by using virtual interfaces (Section 3.3.3). Despite other force-based approaches (e.g. thrust network analysis by Block, 2009), the RBE objective function does not allow handling the value of the forces in particular points directly. This aspect can be addressed

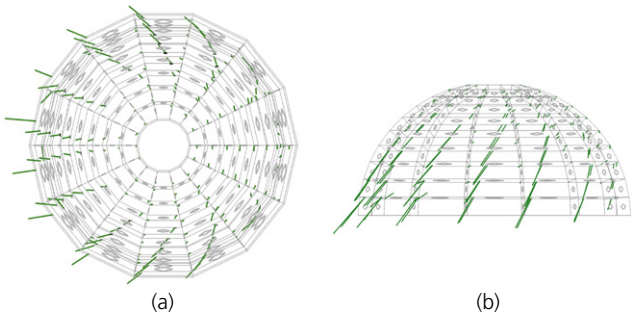

Figure 14. Horizontal capacity analysis: the maximum tilting angle is 32°, obtained with both QP and LP approaches: top view (a) and side-view (b).

by changing the objective function to one that takes only into account the value of the force in certain points (e.g. on the supports) and/or directions (e.g. horizontal, vertical, tangential, etc.). The capacity of the dome subjected to increasing, horizontal static actions has been explored. In this case, the incremental analysis ends because the problem becomes infeasible, and in this case the objective function does not play any role anymore.

4. Discussion

In this section, the main outcome is summarised into two main discussion points.

First, two different objective functions have been proposed and compared, a LP and the original QP, to illustrate the RBE features. The main outcome is that both QP and LP provide statically admissible solutions in the spirit of limit analysis, meaning that there should not be any reason to prefer one to the other. To illustrate this concept, one can observe Figure 4. The two blocks are in contact in four points: it can be possible to interpret the QP and LP results making parallelism with the four-legged stool simply supported on the ground (an example often used to explain the limit analysis approach; Heyman, 1997, 2019). The four-legged stool is a statically indeterminate system and, thus, infinite solutions are possible depending on the actual contact (unknowable) between the table and the ground. The QP solution reported in Figure 4(a) represents an ideal elastic solution, meaning that the contact is assumed to happen in four points. All nodal forces are as much distributed as possible since the objective function is quadratic, which can be correlated with linear elastic interface energy. Conversely, the LP solution presented in Figure 4(b) is just one of the infinite admissible solutions. The equilibrium is guaranteed using only two contact points. Furthermore, looking at the results of Section 3.1, the solution provided by the LP objective function cannot minimise the QP. On the contrary, QP solutions are always solutions to the LP. In this sense, the LP objective

function further widens the space of solutions provided by the QP optimisation. Despite the force distribution is indeterminate, the structure is statically determined if the two blocks assembly globally are considered. The solution in terms of resultants has to be the same regardless of the objective function. As the structural indeterminacy grows up, the solutions of the QP and LP approaches start becoming different from each other (Sections 3.2 and 3.3). The higher the indeterminacy is, the greater the differences are. Indeed, in the dome case, the LP and QP solutions show the highest differences, even in terms of resultants. Finally, if the aim is to select a 'smooth' solution, the QP provides elastic solutions that are as much as possible distributed, which also reflects into symmetric solutions for symmetric models. If the aim is to widen the QP solution space, the LP can provide admissible solutions that are consistent with a perfectly rigid model.

Second, it has been shown that the RBE method can be used to explore different equilibrated states of an indeterminate structure. The concept of new virtual interfaces is utilised, which can be obtained by tightening the original interface and writing the equilibrium constraint on these virtual interfaces. Particularly, introducing the correct definition of the kern of a section, admissible solutions are considered, that can fully activate a set of selected interfaces. This aspect is crucial when the need is to assess the stability of a structure, especially through the estimation of the geometric safety factor. Finally, even if RBE is based on a penalty formulation, it has been demonstrated that this does not affect the search for a limit state. Specifically, when the structure is under a limit condition, the space of solutions may include only one element if the solution is unique (see Sections 3.2.3 and 3.3.3, where tilting test analyses were performed).

5. Conclusion

In this paper, the RBE method has been explored and further developed, paying particular attention to typical masonry assessment problems. RBE is a force-based method that solves the EP through an optimisation process where the objective function minimises the total amount of interface forces and the constraints are represented by linear relations enforcing the static equilibrium and the friction failure conditions. It is worth pointing out that tensile forces are allowed even though highly penalised: in this sense, RBE enlarges the space of admissible stress states. Currently, RBE is implemented in COMPAS (Van Mele *et al*., 2017) and it is an open-source, Python-based package within the COMPAS Masonry framework (Iannuzzo *et al*., 2021). First, the RBE analysis of two simple benchmark cases has been performed to show the meaning of the nodal contact forces and to illustrate how the friction capacity is handled. Second, the same buttressed arch proposed in Iannuzzo *et al*. (2020) has been analysed to benchmark and illustrate the potential of RBE clearly. Finally, a dome with an oculus has been considered, to show how RBE can be used to assess 3D structures also. The main insights of the current research study are the following:

- the kern of a generic polygonal interface has been introduced as a primal variable in the optimisation process. Its use allows to assess and define the range of external actions for which the structure or its part is fully working in compression;
- how to use RBE to explore different internal admissible stress states by virtually reducing the interface (e.g. to its kern) is highlighted. This is a key aspect of RBE method, since it leaves the problem feasible as the virtual reduction does not affect the feasibility of the problem, and in this sense, RBE returns as a solution the one that best matches the prescribed requirement;
- furthermore, since RBE implicitly takes the thickness of the assembly into account, it provides a larger range of statically admissible solutions when compared with methods that use compressive 2D or one-dimensional elements;
- the main differences in using a *friction-net* and *friction+* approach are highlighted and it is shown how the friction-net approach can be more useful when the aim is to evaluate ultimate states ruled by the friction capacity (e.g. 3D mechanisms, Section 3.3.3); and,
- to understand the rule of the nodal forces, all analyses are performed and compared using the original quadratic objective function and a linear one. They both provide admissible stress states but the difference among them increases as the dimension of the graph network, as thus also indeterminacy of problem increases. The quadratic formulation considers the distribution of the nodal forces as much as possible and it comes from an elastic interpretation of the contact among blocks, whereas the linear one considers interface as a rigid element.

The main outcome of this paper is that both QP and LP approaches provide statically admissible solutions in the sense of limit analysis. Since in reality, it is hopeless to try to understand the actual contact condition, there is no reason to prefer one to another, being each solution a possible admissible stress state. Unless one has to face very large problems, for which LP solutions are more affordable (i.e. less time consuming). In this light, RBE is a powerful tool that can be used to explore a wide range of equilibrium states and corresponding stress solutions and its use allows tackling typical masonry assessment problems properly.

Acknowledgements

This study was supported by the NCCR DFAB (National Centre of Competence in Research in Digital Fabrication in

Architecture) funded by the Swiss National Science Foundation (project number 51NF40-141853) and by the SNSF – Swiss National Science Foundation (Project number 178953: 'Practical Stability Assessment Strategies for Vaulted Unreinforced Masonry Structures').

REFERENCES

Angelillo M and Fortunato A (2004) Equilibrium of masonry vaults. In *Novel Approaches in Civil Engineering. Lecture Notes in Applied and Computational Mechanics* (Frémond M and Maceri F (eds)). Springer, Berlin, Heidelberg, Germany, vol. 14, pp. 105–111, https://doi.org/10.1007/978-3-540-45287-4_6.

Angelillo M, Cardamone L and Fortunato A (2010) A numerical model for masonry-like structures. *Journal of Mechanics of Materials and Structures* **5(4)**: 583–615, https://doi.org/10.2140/jomms.2010.5.583.

Angelillo M, Fortunato A, Gesualdo A *et al.* (2018) Rigid block models for masonry structures. *International Journal of Masonry Research and Innovation* **3(4)**: 349–368, https://doi.org/10.1504/IJMRI.2018.095701.

Block P (2009) *Thrust Network Analysis: Exploring Three-Dimensional Equilibrium*. Doctoral dissertation, Massachusetts Institute of Technology, Boston, MA, USA.

Block P and Lachauer L (2014) Three-dimensional funicular analysis of masonry vaults. *Mechanics Research Communications* **56**: 53–60, https://doi.org/10.1016/j.mechrescom.2013.11.010.

Block P and Ochsendorf JA (2007) Thrust network analysis: a new methodology for three-dimensional equilibrium. *Journal of the International Association for Shell and Spatial Structure* **48(3)**: 167–173.

Block P, Ciblac T and Ochsendorf JA (2006a) Real-time limit analysis of vaulted masonry buildings. *Computers & Structures* **84(29-30)**: 1841–1852, https://doi.org/10.1016/j.compstruc.2006.08.002.

Block P, DeJong MJ and Ochsendorf JA (2006b) As hangs the flexible line: equilibrium of masonry arches. *Nexus Network Journal* **8(2)**: 13–24, https://doi.org/10.1007/s00004-006-0015-9.

Bullet-Physics-Library (2012) (Copyright © 2012) Bullet collision detection and physics library. http://bulletphysics.org.

Como M (2013) *Statics of Historic Masonry Constructions*. Springer, Berlin, Heidelberg, Germany.

CPLEX II (2009) *V12. 1: User's Manual for CPLEX*. International Business Machines Corporation, Armonk, NY, USA, vol. 46, (53), p. 157.

Cundall PA (1971) A computer model for simulating progressive large scale movements in blocky rock systems. In *Proceedings of the International Symposium on Rock Mechanics, Nancy, France*.

D'Ayala D and Casapulla C (2001) Limit state analysis of hemispherical domes with finite friction. In *Historical Constructions, Possibilities of Numerical and Experimental Techniques, Guimarães* (Lourenço P.B. and Roca P. (eds)), pp. 617–626.

De Chiara E, Cennamo C, Gesualdo A *et al.* (2019) Automatic generation of statically admissible stress fields in masonry vaults. *Journal of Mechanics of Materials and Structures* **14(5)**: 719–737, https://doi.org/10.2140/jomms.2019.14.719.

Diamond S and Boyd S (2016) CVXPY: a Python-embedded modeling language for convex optimization. *The Journal of Machine Learning Research* **17(1)**: 2909–2913, https://doi.org/10.5555/2946645.3007036.

Fraternali F (2010) A thrust network approach to the equilibrium problem of unreinforced masonry vaults via polyhedral stress functions. *Mechanics Research Communications* **37(2)**: 198–204, https://doi.org/10.1016/j.mechrescom.2009.12.010.

Fraternali F, Angelillo M and Fortunato A (2002) A lumped stress method for plane elastic problems and the discrete-continuum approximation. *International Journal of Solids and Structures* **39(25)**: 6211–6240, https://doi.org/10.1016/S0020-7683(02)00472-9.

Frick U, Van Mele T and Block P (2015) Decomposing three-dimensional shapes into self-supporting, discrete-element assemblies. *Modelling Behaviour* 187–201, https://doi.org/10.1007/978-3-319-24208-8_16.

Frick U, Van Mele T and Block P (2016) Data management and modelling of complex interfaces in imperfect discrete-element assemblies. In *Proceedings of the IASS Annual Symposia. International Association for Shell and Spatial Structures (IASS)*, vol. 17, pp. 1–9.

Gesualdo A, Brandonisio G, De Luca A *et al.* (2019) Limit analysis of cloister vaults: the case study of Palazzo Caracciolo di Avellino. *Journal of Mechanics of Materials and Structures* **14(5)**: 739–750, https://doi.org/10.2140/jomms.2019.14.739.

Gilbert M and Melbourne C (1994) Rigid-block analysis of masonry structures. *Structural Engineer* **72(21)**: 356–361.

Gilbert M, Casapulla C and Ahmed HM (2006) Limit analysis of masonry block structures with non-associative frictional joints using linear programming. *Computers & Structures* **84(13–14)**: 873–887, https://doi.org/10.1016/j.compstruc.2006.02.005.

Hally D (1987) *Calculation of the Moments of Polygons*. Defence Research Establishment Suffield, Ralston, AB, USA.

Heyman J (1966) The stone skeleton. *International Journal of Solids and Structures* **2(2)**: 249–279, https://doi.org/10.1016/0020-7683(66)90018-7.

Heyman J (1969) The safety of masonry arches. *International Journal of Mechanical Sciences* **11(4)**: 363–385, https://doi.org/10.1016/0020-7403(69)90070-8.

Heyman J (1997) *The Stone Skeleton: Structural Engineering of Masonry Architecture*. Cambridge University Press, Cambridge, UK.

Heyman J (2019) The structural engineer's view of ancient buildings. *Journal of Mechanics of Materials and Structures* **13(5)**: 609–615, https://doi.org/10.2140/jomms.2018.13.609.

Huerta S (2006a) Galileo was wrong: the geometrical design of masonry arches. *Nexus Network Journal* **8(2)**: 25–52, https://doi.org/10.1007/s00004-006-0016-8.

Huerta S (2006b) Geometry and equilibrium: the gothic theory of structural design. *The Structural Engineer* **84(2)**: 23–28.

Iannuzzo A (2019) Energy based fracture identification in masonry structures: the case study of the church of 'Pietà dei Turchini'. *Journal of Mechanics of Materials and Structures* **14(5)**: 683–702, https://doi.org/10.2140/jomms.2019.14.683.

Iannuzzo A, De Luca A, Fortunato A, Gesualdo A and Angelillo M (2018) Fractures detection in masonry constructions under horizontal seismic forces. *Ingegneria Sismica* **35(3)**: 87–103.

Iannuzzo A, Van Mele T and Block P (2020) Piecewise rigid displacement (PRD) method: a limit analysis-based approach to detect mechanisms and internal forces through two dual energy criteria. *Mechanics Research Communications* **107**: 103557, https://doi.org/10.1016/j.mechrescom.2020.103557.

Iannuzzo A, Dell'Endice A, Maia Avelino R *et al.* (2021) COMPAS masonry: a computational framework for practical assessment of unreinforced masonry structures. In *Proceedings of the SAHC Symposium, Barcelona*.

Livesley RK (1978) Limit analysis of structures formed from rigid blocks. *International Journal for Numerical Methods in Engineering* **12(12)**: 1853–1871, https://doi.org/10.1002/nme.1620121207.

Livesley RK (1992) A computational model for the limit analysis of three-dimensional masonry structures. *Meccanica* **27(3)**: 161–172, https://doi.org/10.1007/BF00430042.

Mousavian E and Casapulla C (2020) The role of different sliding resistances in limit analysis of hemispherical masonry domes. *Frattura ed Integrità Strutturale* **14(51)**: 336–355, https://doi.org/10.3221/IGF-ESIS.51.25.

Nvidia Physx Library (2013) See http://www.nvidia.com/object/physx-9.12.0213-driver.html.

Ochsendorf JA (2002) *Collapse of Masonry Structures*. Doctoral dissertation, University of Cambridge, Cambridge, UK.

Orduña A and Lourenço PB (2005) Three-dimensional limit analysis of rigid blocks assemblages. Part I: torsion failure on frictional interfaces and limit analysis formulation. *International Journal of Solids and Structures* **42(18-19)**: 5140–5160, https://doi.org/10.1016/j.ijsolstr.2005.02.010.

Portioli F, Casapulla C, Gilbert M and Cascini L (2014) Limit analysis of 3D masonry block structures with non-associative frictional joints using cone programming. *Computers & Structures* **143**: 108–121, https://doi.org/10.1016/j.compstruc.2014.07.010.

Portioli F, Casapulla C and Cascini L (2015) An efficient solution procedure for crushing failure in 3D limit analysis of masonry block structures with non-associative frictional joints. *International Journal of Solids and Structures* **69**: 252–266, https://doi.org/10.1016/j.ijsolstr.2015.05.025.

Romano G (2002) *Scienza Delle Costruzioni*. Hevelius, Benevento, Italy.

Van Mele T, Casas G, Rust R *et al.* (2017) COMPAS: a framework for computational research in architecture and structures. https://doi.org/10.5281/zenodo.2594510, http://compas-dev.github.io/.

Whiting EJW (2012) *Design of Structurally-Sound Masonry Buildings Using 3D Static Analysis*. Doctoral dissertation, Massachusetts Institute of Technology, Boston, MA, USA.

Whiting E, Ochsendorf JA and Durand F (2009) Procedural modeling of structurally-sound masonry buildings. In *ACM SIGGRAPH Asia 2009 Papers*, pp. 1–9.